Inorganic Chemistry

Article

pubs.acs.org/IC

Structure, Bonding, and Catecholase Mechanism of Copper Bispidine Complexes

Peter Comba,* Bodo Martin, Amsaveni Muruganantham, and Johannes Straub

Universität Heidelberg, Anorganisch-Chemisches Institut, INF 270, D-69120 Heidelberg, Germany

Supporting Information

ABSTRACT: Oxygen activation by copper(I) complexes with tetra- or pentadentate mono- or dinucleating bispidine ligands is known to lead to unusually stable *end-on*-$[\{(\text{bispidine})\text{Cu}\}_2(O_2)]^{2+}$ complexes (bispidines are methyl-2,4-bis(2-pyridin-yl)-3,7-diazabicyclo-[3.3.1]-nonane-9-diol-1,5-dicarboxylates); catecholase activity of these dinuclear $Cu^{II/I}$ systems has been demonstrated experimentally, and the mechanism has been thoroughly analyzed. The present density functional theory (DFT) based study provides an analysis of the electronic structure and catalytic activity of $[\{(\text{bispidine})\text{Cu}\}_2(O_2)]^{2+}$. As a result of the unique square pyramidal coordination geometry, the $d_{x^2-y^2}$ ground state leads to an unusual σ/π bonding pattern, responsible for the stability of the peroxo complex and the observed catecholase activity with a unique mechanistic pathway. The oxidation of catechol to *ortho*-quinone (one molecule per catalytic cycle and concomitant formation of one equivalent of H_2O_2) is shown to occur via an associative, stepwise pathway. The unusual stability of the *end-on*-peroxo-dicopper(II) complex and isomerization to copper(II) complexes with chelating catecholate ligands, which inhibit the catalytic cycle, are shown to be responsible for an only moderate catalytic activity.

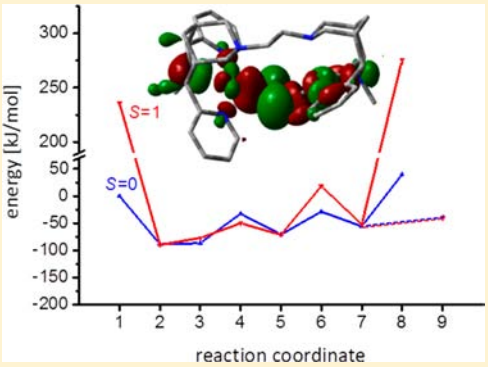

INTRODUCTION

Copper is an important element in biological[1−7] and industrial[8−10] oxidation processes, and copper proteins perform a variety of physiological functions, including the transport of electrons and dioxygen, as well as oxidation and oxygenation processes.[11] Copper in mono- and oligonuclear complexes assists electron transfer via its Cu^I and Cu^{II} oxidation states, and the function of copper enzymes is often based on the reversible binding of molecular dioxygen by one or more Cu^I centers, in combination with electron transfer, to form a variety of copper superoxo, peroxo, and oxo adducts.[1−7,12,13] Among the structurally diverse complexes the two isomeric *trans*-μ-1,2-peroxo-dicopper(II) (*end-on*-$[Cu_2O_2]^{2+}$) and μ-η^2:η^2-peroxo-dicopper(II) complexes (*side-on*-$[Cu_2O_2]^{2+}$) are relevant intermediates for catechol oxidase and related model systems such as those discussed here.[14−16]

Catechol oxidase is an enzyme with a type-3 dicopper active site that catalyzes the oxidation of a range of *ortho*-diphenol (catechol) substrates to the corresponding *ortho*-quinones (see Scheme 1). These quinones may undergo polymerization to afford the brown polyphenolic pigment melanin, which protects damaged tissues against pathogens or insects.[6,17] Catechol oxidase was first isolated in 1937, and the X-ray crystallographic characterization of catechol oxidase, isolated from sweet potatoes, was reported in 1998.[17−19] A large number of low molecular weight model complexes were developed to help to understand the active site geometric and electronic structures and to mimic the catalytic reactivity, and this was supported by various computational studies.[12,20−25] Much of this work has been reviewed.[23,26,27]

The enzyme mechanism, based on experimental data and supported by computational work, is shown in Scheme 2.[5,25,27−30] It consists of four steps, involving (i) the reaction of the resting state (Cu^{II}-OH-Cu^{II}, met) with a substrate molecule to form a metastable intermediate with a catecholate coordinated to the dicopper(II) site, (ii) the formation of the first *ortho*-quinone and a water molecule, (iii) the binding of a dioxygen molecule and a second catechol to the emerging unbridged dicopper(I) species, resulting in a *side-on*-$[Cu_2O_2]^{2+}$ intermediate with a catecholate coordinated to the dicopper-(II)peroxo site, and (iv) the release of the second *ortho*-quinone and a second water molecule after electron transfer, to regenerate the resting state. That is, in each catalytic cycle, two *ortho*-quinone molecules and two molecules of water (from O_2) are produced.[31]

Scheme 1. Catecholase Reaction[a]

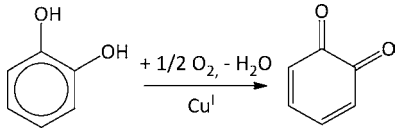

[a]The reduced oxygen species, H_2O or H_2O_2, are omitted.

Received: March 5, 2012
Published: August 21, 2012

   dx.doi.org/10.1021/ic3004917 | *Inorg. Chem.* 2012, 51, 9214−9225

Scheme 2. (a) Enzyme Catecholase Mechanism with Two Catechol Molecules Oxidized to *ortho*-Quinone and One O_2 Reduced to Two Molecules of Water Per Cycle; (b) the bispidine-Based Model, Where One *ortho*-Quinone Is Produced Per Cycle and One O_2 Is Reduced to H_2O_2[16]

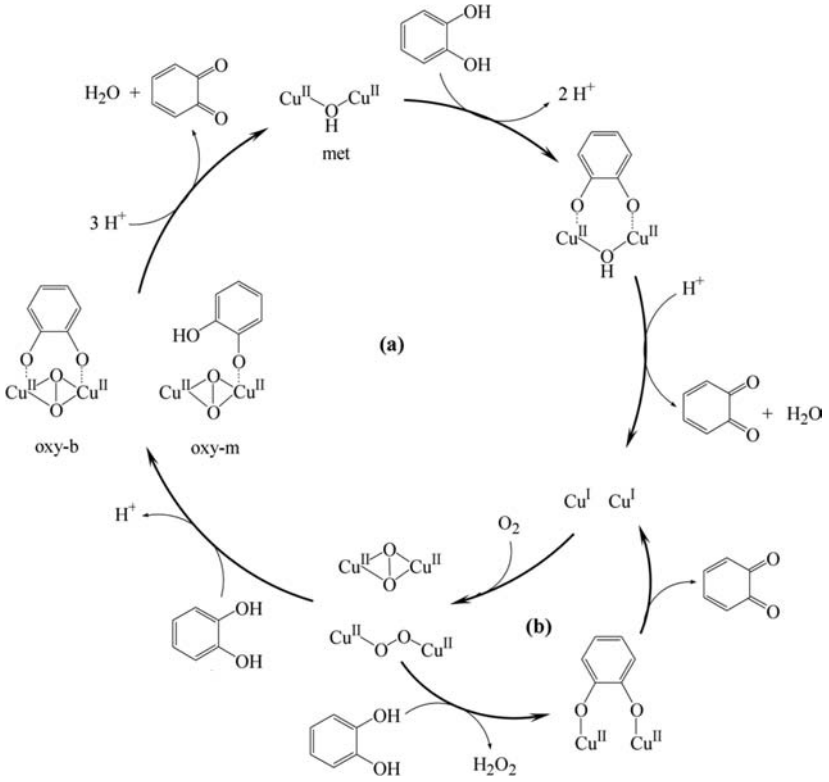

Modeling of catecholase activity with low molecular weight copper complexes has produced a range of structural models, including *end-on*-$[Cu_2O_2]^{2+}$ as well as *side-on*-$[Cu_2O_2]^{2+}$,[1,32−34] the catecholase met-intermediate (see Scheme 2)[26,35] and copper catecholate complexes with mono-, bidentate, and bridging catecholates.[15,36−38] The electronic structure and spectroscopy of some of these biomimetic compounds has been studied in detail.[39,40] A large number of mechanistic studies on model systems have been reported, and these include the analysis of structure-activity relationships, specifically the correlation of pH profiles, redox potentials, and structural parameters with the catecholase activity, as well as a large amount of thorough kinetic work.[41−53] As a result, catalytic cycles for some of the biomimetic systems were proposed, and there are two main classes of catalysts with strikingly different catalytic pathways (see Scheme 2): while there are "true" biomimetic systems with the production of two *ortho*-quinones and two water molecules per cycle (a), there also exist efficient catalysts with the production of one *ortho*-quinone and one molecule of hydrogen peroxide per cycle (b);[16,46,47] in many cases, however, the detailed mechanism has not been studied.

Upon oxygenation, copper(I) bispidine complexes are known to form unusually stable *end-on*-$[Cu_2O_2]^{2+}$ complexes and, for steric reasons, *side-on*-$[Cu_2O_2]^{2+}$ species are less favored.[14,16,54,55] Tetra- and pentadentate bispidine ligands of the type shown in Scheme 3 are extremely rigid and enforce *cis*-octahedral or square pyramidal geometries with very strong in-plane substrate binding,[54,56−60] and dinucleating ligands with optimized linker size and geometry have been used to increase the stability of the dicopper(II) centers.[14,32,54,55] These dinuclear copper complexes have been shown to be active catecholase model systems, and the catalytic pathway was shown to involve only one catechol/*ortho*-quinone pair and the reduction of dioxygen to hydrogen peroxide (mechanism (b) in Scheme 2).[15,16] We now report quantum-chemical studies, based on density functional theory (DFT), to elucidate the electronic structure and bonding of the *end-on*-$[Cu_2O_2]^{2+}$ species and probe the proposed catalytic cycle.

Scheme 3. Bispidine-Based Ligands Tested for Catecholase Activity[16]

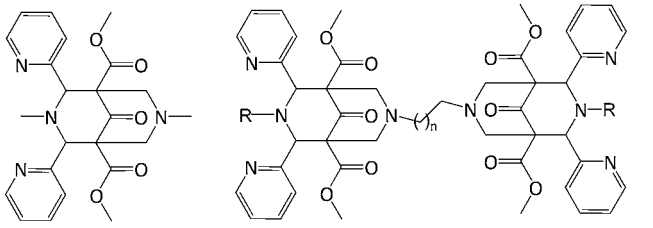

COMPUTATIONAL DETAILS

For simplicity, the structural model used in all calculations was slightly modified from the actual complex: the ester groups in positions 1 and 5 as well as the keto group in position 9 of the bispidine ligands (see Scheme 3) were replaced by H atoms. Most of the DFT calculations were performed with the software package ORCA [version 2.9.1],[61,62] with the B3LYP functional[63−65] and the def2-TZVP basis set for Cu, N, O and def2-SVP for C and H (BS1).[66,67] For some preliminary tests and a comparative study of DFT functionals, the software package Jaguar 6.5[68] was used (see Supporting Information). Initial studies of the reaction pathway were done with Gaussian 09[69] with the B3LYP functional and the LANL2DZ basis set (BS2);[70−72] these data,

dx.doi.org/10.1021/ic3004917 | Inorg. Chem. 2012, 51, 9214−9225

Table 1. Selected B3LYP-Computed (ORCA/BS1) and Experimental Structural Parameters for $[(L^2)Cu_2(O_2)]^{2+}$ and $[(tmpa)_2Cu_2(O_2)]^{2+}$ (Open-Shell Singlet and Triplet States) in Comparison with Experimental Structural Data[a]

	distances [Å]						angles [deg]		dihedrals [deg]	
	Cu−O		Cu−Cu		O−O		Cu−O−O		Cu−O−O−Cu′	
	$S = 0$	$S = 1$	$S = 0$	$S = 1$	$S = 0$	$S = 1$	$S = 0$	$S = 1$	$S = 0$	$S = 1$
				$[(tmpa)_2Cu_2(O_2)]^{2+}$						
X-ray	*1.87*		*4.48*		*1.45*		*111.5*		*180.0*	
calc gas phase	1.93		4.43		1.37		114.9		138.8	
calc, MeCN	1.92		4.36		1.39		114.0		133.7	
calc dispersion	1.91		4.22		1.37		113.3		123.8	
calc MeCN, dispersion	1.91	1.92	4.11	4.09	1.38	1.37	115.7	116.2	106.6	103.9
calc MeCN, dispersion fixed Cu−O−O−Cu	1.88	1.89	4.39	4.37	1.42	1.44	106.8	105.5	180.0	180.0
				$[(L^2)Cu_2(O_2)]^{2+}$						
MM	*1.83*		*4.42*		*1.47*		*109.5*		*152.5*	
calc MeCN, dispersion	1.90	1.90	4.25	4.23	1.41	1.40	112.1	113.3	128.3	123.0

[a]The averages of the two Cu−O distances and Cu−O−O angles are given for all structures.

Scheme 4. Schematic Representation of the π^*_σ Bonding and Antibonding Interactions[a] in $[(L^2)Cu_2(O_2)]^{2+}$ and $[(tmpa)_2Cu_2(O_2)]^{2+}$; the π^*_v Interaction[b] Is Not Shown

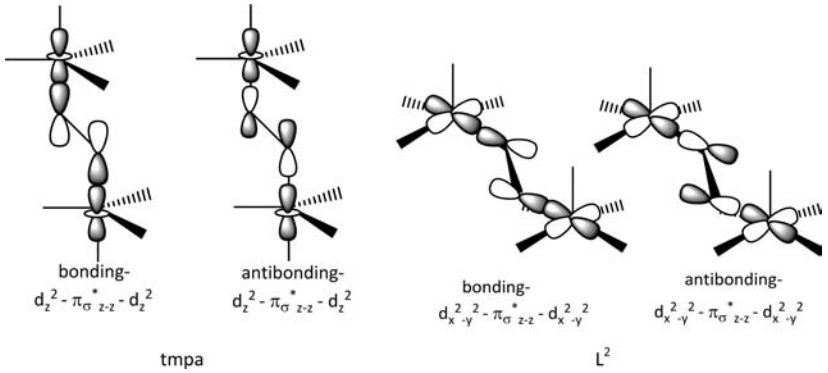

[a]In plane with the σ-type Cu^{II}-O_2 MO.

[b]Vertical O_2-based MO interacting with Cu^{II}.

both gas phase calculations and calculations with implicit solvent treatment, but without empirical dispersion corrections, are shown for comparison as Supporting Information. For the open-shell singlet calculations, the broken symmetry approach as implemented in ORCA (via the "flipspin" procedure) was used. All calculations use empirical dispersion corrections (D3 in ORCA)[73−75] and the COSMO[76] solvent model for acetonitrile. Because analytical frequencies are not available in ORCA, we were unable to perform frequency calculations (enthalpic, free energy and ZPE corrections at $T = 298.15$ K) as the numerical procedure is prohibitively time-consuming. Therefore, we report the values for the corresponding frequency calculations on the Gaussian09-optimized structures with BS2. For most structures the energy differences between the two methods and the structural differences are very small (see the Supporting Information for the corresponding overlay and reaction profile plots). In the discussion below, we will focus on the ORCA calculations; the complete results of the Gaussian09 calculations are also given as Supporting Information.

The importance of including dispersion corrections for the calculation of systems of the type studied here is well established.[77] However, in the present case and in particular with the tmpa-based system (tmpa = tris(2-methylpyridyl)amine), this leads to problems, which in fact are also apparent with solvation included in the Gaussian09 calculations. In the tmpa-based end-on peroxo-dicopper(II) complex, which is known to have a Cu−O−O−Cu dihedral angle of 180°,[33] the $\pi-\pi$ interactions between two pyridine groups coordinated to one of the two Cu^{II} centers each lead to the stabilization of a conformation with a smaller torsion (down to less than 110° when the solvent is treated implicitly via COSMO, see below). It appears that the subtle balance between ligand-based steric effects, metal-based electronic preferences and secondary interactions is not well enough tuned in this case. However, since dispersion is expected to be of importance for the interaction of the complexes with catechol and the stepwise oxidation,[77] dispersion and solvation were included with a fixed dihedral angle in the case of the tmpa-based system (see Supporting Information for details). With the L^2-based complexes this is not a problem because the more rigid ethylene bridge prevents such a folding of the peroxo-bridged structure.

For the calculation of the electronic spectra, time-dependent DFT (TD-DFT) calculations were performed with ORCA and the def2-TZVP[67] basis set for all atoms. For both the antiferromagnetically coupled open-shell singlet ($S = 0$) and the ferromagnetically coupled triplet ($S = 1$) states, where each of the unpaired electrons on the Cu centers couples with one O−O π^* orbital, Gibbs free energies (including ZPE corrections, from the Gaussian 09 calculations) are included in the reaction profiles, since entropic interactions are of importance in the catecholase process. As nomenclature in the text we generally use a simplified form of the stoichiometric formulas, preceded by a superscript for the spin state and succeeded by a subscript which indicates, whether or not solvation was used in the calculations, for example, $^3[(L^2)Cu_2O_2]_g$ for the gas phase structure of the L^2-based *end-on* Cu^{II} peroxo complex on the triplet surface (the subscript *an* is used for solvation with acetonitrile). The expectation values for $\langle S^2 \rangle$ are given for all intermediates and transition states.

There is detailed literature on DFT and TD-DFT applied to copper-dioxygen systems, and this has been reviewed.[23] In addition, there is a recent benchmark study on CuO^+,[78] and this is of interest in

dx.doi.org/10.1021/ic3004917 | Inorg. Chem. 2012, 51, 9214−9225

the context of the work discussed here and also in relation to recent experimental work with similar systems.[79] The copper systems discussed here are open-shell molecules with multideterminantal characteristics, which require a careful evaluation of the choice of the DFT method. The reasonably good performance of the B3LYP hybrid functional for this kind of study is well documented.[80−86] A major problem, however, is that the triplet state tends to be overstabilized with B3LYP, and the coupling constant J therefore is underestimated, that is, there are cases where B3LYP fails to predict the correct spin state ordering in comparison with experiment and with high level CASPT2 calculations.[86] An example of some relevance for the present study is the failure of DFT (BLYP) to predict the correct ground state of the copper(III) peroxide-copper(II) superoxide equilibrium in mononuclear copper complexes with a β-diketiminate ligand backbone.[87−89] In most cases, the expected error limit in energies due to B3LYP calculations is in the range of 10−20 kJ.[90]

The quantum-chemical model used for our analysis has been validated based on the experimental structures of the tmpa- and bn_3tren-based systems (bn_3tren = tris(ethylbenzylamine)amine) as well as with the MM-optimized structure of our L^2-based complex (see Supporting Information), that is, the model chemistry with B3LYP and the BS1 and BS2 basis sets for general structure optimization is expected to produce results with reasonable accuracy. The significant differences between the observed or MM-derived structural parameters and those of the DFT-optimized structures (see Table 1) are not critical and not unexpected,[91−93] and the important structural features which are expected to be of importance for the spectroscopy and reactivities, are well reproduced: the *end-on*-$[Cu_2O_2]^{2+}$ complex with tmpa has three pyridine and one tertiary amine donors, arranged in a trigonal bipyramidal geometry with the peroxo group in an axial position, while the bispidine-based complexes have a bis-pyridine-bis-tertiary amine donor set with a square pyramidal geometry around the Cu^{II} centers and the peroxo group in-plane, with an axial tertiary amine donor (see also Scheme 4).

The treatment of solvation (using COSMO with MeCN, see above) was problematic. The calculations of the peroxo complexes of L^2 and tmpa as well as the reaction coordinate of the L^2- based complex with catechol were done both on the open-shell singlet (S = 0) and triplet (S = 1) spin surfaces, with acetonitrile as implicit solvent and with empirical dispersion corrections (ORCA/BS1), and also with Gaussian09/BS2 in the gas phase and with solvation (see Supporting Information). As outlined above, the solvent and dispersion-corrected calculations of the tmpa- (and L^2-) based complexes lead to an artificial distortion of the geometry, mostly in the Cu−O−O−Cu dihedral and specifically with $[(tmpa)_2Cu_2O_2]^{2+}$, and this critically influences the d orbital energies and mixing of the d orbital coefficients for bonding to the peroxo bridge. For $^1[(tmpa)_2Cu_2O_2]^{2+}$ with solvent and dispersion corrections, the Cu−O−O−Cu dihedral is only 107°, which is a large deviation from 180° observed in the crystal structure. Using only dispersion, we find the dihedral is 124°, with implicit solvent only 134°, and 139° in the gas phase calculation. Including one or both of the corrections also shortens the O−O bond to 1.38 Å (compared to 1.45 Å in the crystal structure), and the Cu···Cu distance to 4.36−4.11 Å (compared to 4.48 Å in the crystal structure). Constraining the Cu−O−O−Cu dihedral to 180° "fixes" these problems, and the Cu···Cu and O−O distances are in acceptable agreement with the crystal structure with 4.39 Å and 1.42 Å, respectively. The constrained optimized structure of $^1[(tmpa)_2Cu_2O_2]^{2+}$ for S = 0 is only 0.6 kJ/mol less stable than the relaxed structure (27.2 kJ/mol when also adding the empirical dispersion at the optimized unconstrained geometry). Constraining the Cu−O−O−Cu dihedral also leads to the correct prediction of the S = 0 electronic ground state $^1[(tmpa)_2Cu_2O_2]^{2+}$, which is less stable by 4.4 kJ/mol in the unconstrained calculation.

As the L^2-based system is more rigid than the tmpa-based complex, we do not expect similar problems when solvation and dispersion are included. Therefore, both corrections were included in the calculated reaction profile of the L^2-based system with catechol (without any constraints), as the solvent is expected to have a significant effect on the overall reactivity and catalytic activity.[94] The only exception is in the direct comparison of the tmpa- and L^2-based peroxo complexes, because here the $^1[(L^2)Cu_2O_2]^{2+}$ complex is calculated to be less stable by only 1.4 kJ/mol than the $^3[(L^2)Cu_2O_2]^{2+}$ complex (see below). Also, as it is difficult to judge the effects of the different corrections, we use gas phase structures in the S = 0 open shell singlet spin state for the semiquantitative calculation of the UV−vis spectra via TD-DFT.

The orbitals involved in the Cu−O bond strongly depend on the Cu−O−O−Cu torsion (see also discussion above), and this complicates the analysis of the bonding and electronic transitions. An NBO analysis for the peroxo complexes is inconclusive in terms of the semioccupied atomic orbital; for both tmpa- and L^2-based complexes the semioccupied orbital is predicted to be of $d_{x^2-y^2}$ character. We will instead concentrate on the canonical frontier orbitals for the discussion of the bonding differences between the tmpa- and the L^2-based systems (see Supporting Information for plots of the molecular orbitals (MOs) and their energy). The expectation values for S^2 for all intermediates and transition states are also given as Supporting Information.

RESULTS AND DISCUSSION

1. Structure and Bonding of the *trans*-μ-1,2-Peroxo-dicopper(II) Complexes. Although *side-on*-$[Cu_2O_2]^{2+}$ and bis(μ-oxo)-dicopper(III) complexes generally are the active species in the copper-induced oxygen activation of biological systems, *end-on*-$[Cu_2O_2]^{2+}$ complexes are of importance as possible intermediates in the formation of these dicopper-dioxygen species[2,5−7] and, in model systems, they also have been shown to be able to activate C−H bonds.[95] Because of the intrinsic instability of copper-dioxygen adducts the choice of ligand is important. Several *end-on*-$[Cu_2O_2]^{2+}$ complexes have been reported, but X-ray structural data are only available for the tmpa-, bn_3tren-, and Me_6tren-based systems [tmpa = tris(2-methylpyridyl)amine; bn_3tren = tris(ethylbenzylamine)amine; Me_6tren = tris(ethyl-dimethylamine)amine].[33,95,96] With the bispidine ligand systems, the oxygenation of the Cu^I precursor complexes has been studied in detail, and the formation and spectroscopic characterization of stable *end-on*-$[Cu_2O_2]^{2+}$ complexes has been reported.[14,55] The dinucleating ethyl-bridged ligand L^2 (see Scheme 3) was found to form the (to date) most stable *end-on*-$[Cu_2O_2]^{2+}$ complex with a half-live of $t_{1/2}$ = 50 min at ambient temperature.[14,55] The increase in stability with respect to the system with the mononucleating ligand L^1 ($t_{1/2}^{250K}$ = 15 s) was shown to be accompanied by spectroscopic changes and, therefore, not to be solely an entropic effect but also due to subtle structural changes; relatively large changes in stability and spectroscopy are also observed with respect to the tmpa-based system.[6,36] The stability of the bispidine-type systems was proposed to be due to the enforced square pyramidal geometry with an in-plane peroxo group,[14,54,55] and the ligand preorganization for the peroxo-dicopper(II) product by the dinucleating ligand L^2 was shown by molecular mechanics (MM) calculations to induce an additional stabilization of approximately 50 kJ/mol, in good agreement with experiment.[14] This is supported by the observation that the second generation bispidine ligands which enforce a strikingly different coordination geometry to the peroxo-dicopper(II) complexes (distorted trigonal bipyramidal vs. square pyramidal),[59] have a strikingly different copper-dioxygen chemistry.[60]

A simple ligand field analysis predicts the unpaired electron in the d_{z^2} orbital in the trigonal bipyramidal structure of the tmpa complex, and in the $d_{x^2-y^2}$ orbital in the square pyramidal geometry of the bispidine-based *end-on*-$[Cu_2O_2]^{2+}$ complex, and this should lead to significant differences in bonding,

dx.doi.org/10.1021/ic3004917 | Inorg. Chem. 2012, 51, 9214−9225

electronic structure, and spectroscopy. Indeed, while the experimentally observed characteristic charge transfer (CT) transitions of the tmpa-based *end-on*-$[Cu_2O_2]^{2+}$ system ($^1[(tmpa)_2Cu_2O_2]$) are observed at 525 nm (19,047 cm^{-1}) and 590 nm (16,949 cm^{-1}),[36] those of $[(L^2)Cu_2O_2]$ are observed at 486 nm (20,578 cm^{-1}) and 649 nm (15,386 cm^{-1}).[14] The peroxo-dicopper(II) complexes have one unpaired electron on each copper center, and the O−O bridge enables superexchange, leading to a spin-coupled system. The calculation of the triplet $S = 1$ states is straightforward in the DFT formalism (single determinant). The multideterminantal open shell singlet $S = 0$ states were calculated by using one of the two possible antiferromagnetically coupled open-shell singlet states, verified by wave function stability tests, for the Gaussian09 calculations, and the broken-symmetry "flip-spin" procedure for the calculations with ORCA. For both complexes, the structures were optimized in the $S = 1$ and $S = 0$ states. For the *end-on*-$[Cu_2O_2]^{2+}$ complexes, the electronic ground states are $S = 0$ for the tmpa complex, that is, $^1[(tmpa)_2Cu_2O_2]$ (as observed experimentally,[34,39] see Supporting Information), but for $[(L^2)Cu_2O_2]^{2+}$ a triplet electronic ground state is predicted (see below), however, with an energy difference of only 1.4 kJ/mol. This is arguably below the accuracy of the method and basis set combination used (see above), and at room temperature both electronic states should be accessible. For the discussion of the bonding of the two *end-on* peroxo complexes we will therefore and for better comparability focus to a large extent on the $^1[(tmpa)_2Cu_2O_2]$ and $^1[(L^2)Cu_2O_2]$ structures. The computed frontier MO orbital energies of $^1[(tmpa)_2Cu_2O_2]$, $^1[(L^2)Cu_2O_2]$, and $^3[(L^2)Cu_2O_2]$ are given as Supporting Information. The computational analysis of the exchange coupling constant J[5,89,97,98] yields −990.6 cm^{-1} and −390.5 cm^{-1} for the tmpa- and L^2-based peroxo complexes, respectively; that of the tmpa-peroxo dicopper(II) complex is in acceptable agreement with the experimental value of $|J| > 1200$ cm^{-1}.[34] The much smaller value of $|J|$ for the L^2-based complex is as expected from the structural parameters,[99−101] and the more distorted geometry of the L^2-based system is imposed by the nature of the spacer group between the two metal sites.

The Cu^{II} centers in the two systems (tmpa vs L^2) have significantly different electronic configurations. The Cu^{II} ion has a d^9 electronic configuration with an unpaired electron in either the $d_{x^2-y^2}$ or the d_{z^2} orbital. The highest occupied MO (HOMO) of the peroxo-bridge consists of a doubly degenerate set of orbitals, which split upon binding to Cu^{II}. The two degenerate π^* (O−O) frontier orbitals are split into one set in-plane with the σ-type d orbitals, π^*_σ, and one set perpendicular to these d orbitals, π^*_v. The major difference between the bonding pattern of $^1[(tmpa)_2Cu_2O_2]$ and $^{1,3}[(L^2)Cu_2O_2]$ is shown in Scheme 4: while in the tmpa-based system the O_2^{2-}-centered π^*-antibonding MOs overlap in a σ-interaction with the d_{z^2} orbital, in the L^2-based complex $^1[(L^2)Cu_2O_2]$, the corresponding σ-interaction is with the $d_{x^2-y^2}$ metal-based orbital. In the dinuclear $^1[(tmpa)_2Cu_2O_2]$ complex, the two unpaired electrons are coupled antiferromagnetically via superexchange (i.e., the antisymmetric combination $Cu(d_{z^2})$-$Cu(d_{z^2})$ is occupied). In contrast, the interaction of the two Cu^{II}-based singly occupied MOs (SOMOs) of $d_{x^2-y^2}$ character with the oxo bridge π_σ^* and π_v^* orbitals in the square pyramidal complex $[(L^2)Cu_2O_2]$ leads to a symmetric $[Cu(d_{x^2-y^2}) + Cu(d_{x^2-y^2})]$ and an antisymmetric $[Cu(d_{x^2-y^2}) - Cu(d_{x^2-y^2})]$ combination. For $^1[(L^2)Cu_2O_2]_g$, the two unpaired electrons on the Cu^{II} centers occupy the low energy antisymmetric combination and leave a hole in the symmetric combination. In $^3[(L^2)Cu_2O_2]_g$, the antisymmetric combination becomes the HOMO. Because of stronger overlap with the metal orbitals, the π^*_σ orbitals are stabilized more than the π^*_v orbitals. The calculations for $^3[(L^2)Cu_2O_2]$ show frontier orbitals which are qualitatively similar to those of $^1[(L^2)Cu_2O_2]$ (see Supporting Information).

The computed O−O distance for the *end-on*-$[Cu_2O_2]^{2+}$ ($S = 1$) complex $^3[(L^2)Cu_2O_2]_{an}$ is shorter (O−O = 1.40 Å) than in the tmpa-based $^1[(tmpa)_2Cu_2O_2]_{an}$ compound, (O−O = 1.42 Å).[102] The energetically less favorable $^1[(L^2)Cu_2O_2]_{an}$ (+1.4 kJ/mol) has a slightly longer O−O bond 1.41 Å (see Figure 3 and Table 1). The covalency of the σ-Cu^{II}-O bond is similar in the tmpa- and L^2-based peroxo complexes but, while the SOMO of $[(tmpa)_2Cu_2O_2]$ only has one amine donor contribution, that of $[(L^2)Cu_2O_2]$ has one amine and two pyridine donor contributions; the Cu−O bond distances are all very similar: 1.90 Å in $^{1/3}[(L^2)Cu_2O_2]_{an}$ vs 1.88 Å in $^1[(tmpa)_2Cu_2O_2]_{an}$ and 1.89 Å in $^3[(tmpa)Cu_2O_2]_{an}$ (see Table 1). Note that the Cu−O bond length is correlated to the Cu−O−O−Cu dihedral which is for steric reasons significantly smaller in $[(L^2)Cu_2O_2]$ than in $[(tmpa)_2Cu_2O_2]$ (see above; note also that Cu−O−O−Cu is constrained in the calculations of $[(tmpa)_2Cu_2O_2]$; for the unconstrained structures, the Cu−O bond length is 1.91 Å for $^1[(tmpa)_2Cu_2O_2]$ and 1.92 Å for $^3[(tmpa)_2Cu_2O_2]$, that is, longer and weaker than in $[(L^2)Cu_2O_2]$).

The ORCA/BS1 calculations show that the Cu−O bond is significantly shortened when the Cu−O−O−Cu dihedral in $^1[(tmpa)_2Cu_2O_2]$ is constrained to 180° (1.88 Å vs. 1.93−191 Å). If we assume that the solvent and dispersion corrections are (partly) valid for $[(tmpa)_2Cu_2O_2]$, that is, that the actual Cu−O−O−Cu dihedral in solution is less than 180°, then the Cu−O bond in $^1[(tmpa)_2Cu_2O_2]$ is predicted to be shorter than in $[(L^2)Cu_2O_2]$. The expectation of a somewhat stronger Cu−O bond in $^{1,3}[(L^2)Cu_2O_2]$ vs $^1[(tmpa)_2Cu_2O_2]$ is supported by the experimentally observed charge transfer (CT) transitions: the π^*_σ CT band of $[(L^2)Cu_2O_2]$ is shifted to higher energy (20,587 cm^{-1} vs 19,047 cm^{-1} for $[(tmpa)_2Cu_2O_2]$).

2. Electronic Spectra of *end-on*-$[(L^2)Cu_2(O_2)]^{2+}$. For the *end-on*-$[(tmpa)_2Cu_2(O_2)]^{2+}$ complex ($^1[(tmpa)_2Cu_2O_2]$) the X-ray crystal structure is known,[33] and the electronic spectra, with two prominent CT transitions at 525 and 590 nm (19,047 and 16,949 cm^{-1}) and a d-d band at 1,035 nm (9,660 cm^{-1}) have been analyzed in detail.[5,36,39] The transitions can be singlet or triplet, and symmetric or antisymmetric with respect to the two d orbitals of the d^9 copper centers; for $^1[(tmpa)_2Cu_2O_2]$: $\pi^*_\sigma \rightarrow Cu(d_{z^2})$ ($^{1,3}A_g$ and $^{1,3}B_u$) and $\pi^*_v \rightarrow Cu(d_{z^2})$ ($^{1,3}B_g$ and $^{1,3}A_u$). Of these, only the $\pi^*_\sigma \rightarrow Cu(d_{z^2})$ ^1B_u and $\pi^*_v \rightarrow Cu(d_{z^2})$ ^1A_u are electronic dipole and spin-allowed.[5,36,39] The interaction of the π^*_σ orbital with the symmetric d orbital combination stabilizes the π^*_σ orbital, and destabilizes the $d(d_{z^2}) + d(d_{z^2})$ symmetric combination.[5,36,39] For $[(L^2)Cu_2O_2]$ the corresponding orbitals are the $d(d_{x^2-y^2}) - d(d_{x^2-y^2})$ antisymmetric and the $d(d_{x^2-y^2}) + d(d_{x^2-y^2})$ symmetric combinations.

The two observed bands in $[(L^2)Cu_2O_2]$ can be assigned to CT transitions, where the more intense transition at 20,578 cm^{-1} (486 nm) corresponds to $\pi^*_\sigma \rightarrow Cu(d_{x^2-y^2})$ while the less intense shoulder at 15,386 cm^{-1} (649.9 nm) is assigned to the

dx.doi.org/10.1021/ic3004917 | Inorg. Chem. 2012, 51, 9214−9225

$\pi^*_v \rightarrow$ Cu ($d_{x^2-y^2}$) CT transition, in analogy with the tmpa-based system. The experimental spectrum of $^1[(tmpa)_2Cu_2O_2]$ has two transitions at 525 (19,047 cm^{-1}) and 590 nm (16,949 cm^{-1}), as well as a low intensity, low energy transition at 1,035 nm (9,660 cm^{-1}), assigned to a d-d-type $d_{xy},d_{x^2-y^2} \rightarrow d_{z^2}$ transition. A qualitative comparison of $[(L^2)Cu_2O_2]$ with $[(tmpa)_2Cu_2O_2]$ is shown in Figure 1.

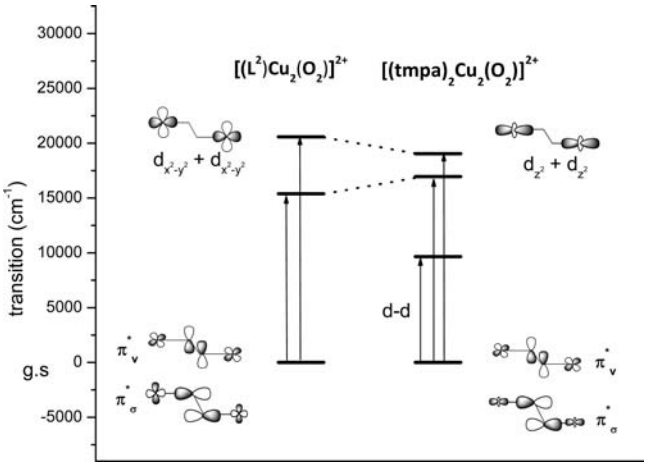

Figure 1. Experimentally observed UV−vis transitions for $[(L)_2Cu_2O_2]^{2+}$ and $[(tmpa)_2Cu_2O_2]^{2+}$, with the corresponding schematic orbital plots.

The electronic spectrum of $^1[(L^2)Cu_2O_2]$ was also computed with TD-DFT (see Computational Details). The spectrum was calculated in both spin states (S = 0, S = 1). Discussed here is only the electronic excitation from the S = 0 singlet state, that of the S = 1 state is given as Supporting Information. The two states are almost isoenergetic, and the fact that the computed spectrum of the singlet state leads to a more accurate prediction of the experimental spectrum supports our choice of the S = 0 state as the electronic ground state (see above); given the accuracy of the DFT method, and the relative stabilities as well as the Cu−O and O−O bond lengths, the population of the S = 0 open shell singlet state is a valid assumption. The computed together with the experimental spectrum and the orbitals involved in the CT transitions are shown in Figure 2. TD-DFT predicts two absorption bands at 405 nm (24,719 cm^{-1}) and

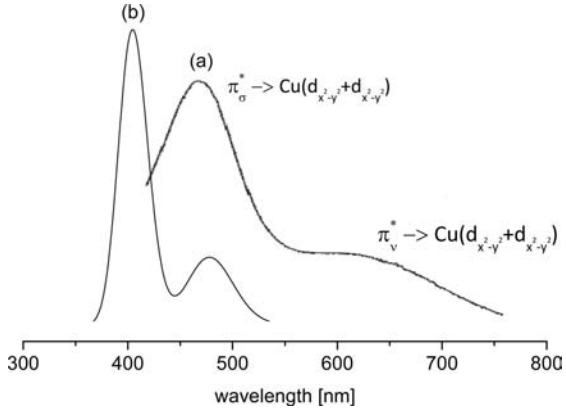

Figure 2. (a) Experimental absorption spectrum (transitions at 20,578 cm^{-1} and 15,386 cm^{-1}); (b) TD-DFT-computed spectrum of $[(L^2)Cu_2O_2]^{2+}$ (transitions at 24,719 cm^{-1} and 20,565 cm^{-1}.

486 nm (20,565 cm^{-1}), which correspond to the $\pi^*_\sigma \rightarrow$ Cu($d_{x^2-y^2}$ + $d_{x^2-y^2}$) and $\pi^*_v \rightarrow$ Cu($d_{x^2-y^2}$ + $d_{x^2-y^2}$) transitions. The energy of the two transitions are overestimated but in acceptable agreement with the experimentally observed transitions.[39,91,103] The calculations predict the π^*_σ transition to be significantly more intense than the π^*_v transition, and this is consistent with the experimental observation.

3. Catecholase Mechanism of the Bispidine Complexes. Copper complexes of the bispidine ligands L^1-L^5 (see Scheme 2) are active catecholase models,[15,16] with the L^5-based complex being the most active catalyst (see Table 2). On the

Table 2. Experimentally Observed Reactivities with Different Bispidine Ligands

	L^1	L^2	L^3	L^4	L^5
k_{cat} [h^{-1}]	0.0	21.5	3.0	0.2	62.0
K_M [mM]		1.04	1.35	11.8	0.07
v_{max} [$\mu M\ s^{-1}$]		0.3	0.04	0.05	0.87

basis of the experimental results, a catalytic cycle (see Scheme 2b) was proposed; the major conclusions were that (i) the bispidine systems are reasonably active catecholase catalysts but the catalytic cycle is not biomimetic, that is, the pathway is strikingly different from that observed in the enzymes;[16] (ii) all individual reaction steps are reasonably efficient, and the overall inefficiency of the reaction is primarily due to product inhibition. The current computational study was performed to check these interpretations. An important feature for the validation of this computational study is the unique set of available structures of the bispidine system which includes all possible coordination modes of catecholate, namely, monodentate, bidentate and bridging.[15]

The main features of the mechanism (see Scheme 2b), proposed on the basis of the experimental data, are as follows: (i) the preorganized dicopper(I) complex binds O_2 to yield a relatively stable *end-on*-$[Cu_2O_2]^{2+}$ complex; (ii) the catechol substrate binds in a bridging mode to yield the $[Cu_2(catecholate)]^{2+}$ complex and one equivalent of H_2O_2; (iii) there is intramolecular electron transfer to form *ortho*-quinone coordinated to the two Cu^I centers; when *ortho*-quinone is released, the catalytically active dicopper(I) species is reformed; (iv) inhibition occurs by formation of a dicopper(II) species with chelating chatecholate(s) in competition with electron transfer in step (iii). Important questions to be answered by our DFT-based analysis are as follows: how do the release of H_2O_2 and the catechol binding proceed in detail (dissociative vs associative mechanism, that is, is the H_2O_2 released before or after catecholate coordination), is catecholate coordination a concerted or a stepwise process, what is the rate limiting step of the entire cycle, and how may the inhibition of product formation be prevented?

All relevant intermediates and transition states are shown in Scheme 5 (the numbering of these species is also used in the reaction profile of Figure 3, and the optimized structures shown in Figure 4).[104] The first step in the catalytic cycle is the formation of *end-on*-$[(L^2)Cu_2O_2]^{2+}$, **2**. The electronic ground state of the precursor $[(L^2)Cu^I_2]^{2+}$, **1**, is S = 0. Energies of the other species are tabulated in Figure 3 relative to **1**. The oxygenation of $[(L^2)Cu^I_2]^{2+}$ with $^3O_2$ leads to *end-on*-$[(L^2)Cu_2O_2]^{2+}$, **2**, for which the S = 1 state is the electronic ground state (see above), that is, at the beginning of the catalytic transformation, there is a spin crossover to the triplet

dx.doi.org/10.1021/ic3004917 | Inorg. Chem. 2012, 51, 9214−9225

Scheme 5. Associative Stepwise and Concerted Pathway for the Catecholase Activity by Bispidine Dicopper Complexes[a]

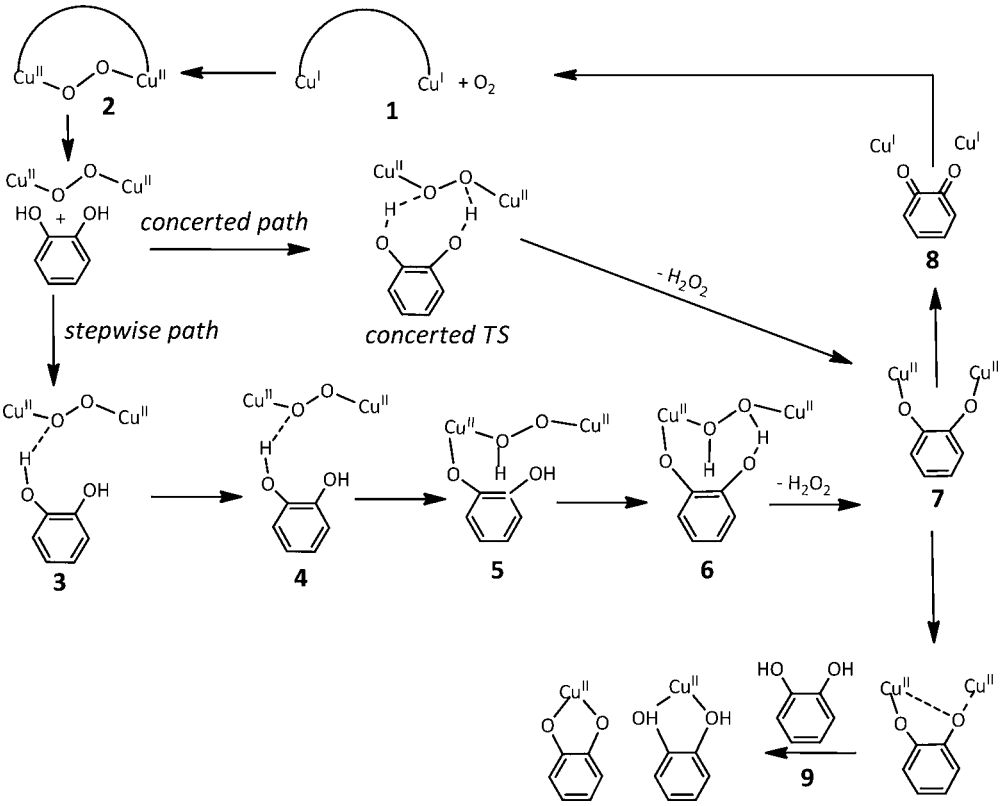

[a]The numbering of the various species is the same as in Figures 3 and 4.

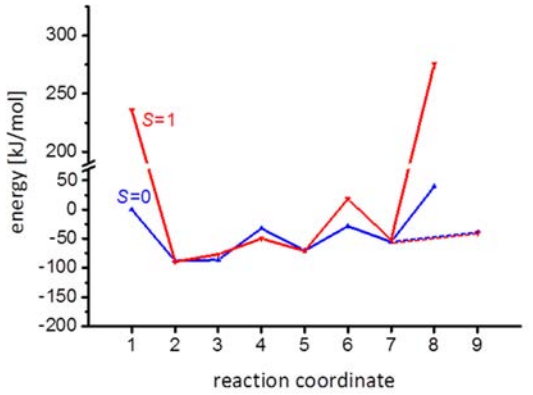

structure No. ΔE [kJ/mol]	1	2	3	4	5	6	7	8	9
$S = 0$	0.0	-88	-87	-32	-71	-29	-56	40	-37
$S = 1$	236	-90	-77	-50	-71	18	-52	276	-41

Figure 3. Top: reaction path profile for the stepwise mechanism of the catechol oxidation by bispidine-dicopper complexes; calculation with implicit solvent (COSMO, solvent = acetonitrile) and empirical dispersion correction, with ORCA/BS1. **1**: $[Cu_2]^{2+}$ + O_2 + catechol, **2**: $[Cu_2(O_2)]^{2+}$ + catechol, **3**: weak complex, **4**: transition state 1, **5**: intermediate 1, **6**: transition state 2, **7**: bridged catechol + H_2O_2, **8**: $[Cu_2]^{2+}$ + H_2O_2 + quinone, **9**: inhibition product (see Scheme 5 for numbering and Figure 4 for the relevant structures); bottom: tabulated final electronic energies.

surface. The reaction from ^{1}**1** to ^{3}**2** is exergonic by 90 kJ/mol. Notably, the S = 0 open shell singlet is only 1.4 kJ/mol less stable. Given the accuracy of the method used, and the possible uncertainties when calculating only one of the two possible singlet states in the single-determinantal DFT methodology, one cannot rule out the population of the S = 0 state at room temperature.[105] Indeed, for all intermediates the two spin states are degenerate within the accuracy of the methods used, and this is a typical example for two-state reactivity.[106,107]

A dissociative mechanism, that is, protonation of the peroxo bridge by catechol, followed by the release of H_2O_2 from *end-on*-$[(L^2)Cu_2(H_2O_2)]^{4+}$ to form H_2O_2 and the hypothetical $[(L^2)Cu^{II}_2]^{4+}$ species, which then reacts with the deprotonated catecholate substrate, is, as expected, a highly unfavorable process. In the alternative associative process, there are two possible pathways by which the catechol substrate binds to the *end-on*-$[Cu_2O_2]^{2+}$ catalytically active form **2**: (i) the two protons from catechol are transferred simultaneously to the two oxygen atoms of the peroxo bridge (concerted mechanism) or (ii) one after the other (stepwise mechanism, see Scheme 5). Both pathways were studied; however, our attempts to compute a concerted pathway were unsuccessful and only asymmetric transition states, which collapsed to the stepwise reaction channel, were found. From potential energy surface scans, we estimate the energy barrier of the concerted mechanism to be about 92 kJ/mol, that is, about 50 kJ/mol less favorable than the stepwise pathway (see Supporting Information; this also includes selected structural parameters and spin densities of the various species discussed here).

It follows from the calculations that catechol approaches the *end-on*-$[Cu_2O_2]$ complex **3**, protonates the peroxo bridge in a stepwise process (**4**-**5**-**6**), and binds to the dicopper(II) complex **7**, which then releases H_2O_2 (see Scheme 5). This pathway is now discussed in detail. When catechol approaches

dx.doi.org/10.1021/ic3004917 | *Inorg. Chem.* 2012, 51, 9214−9225

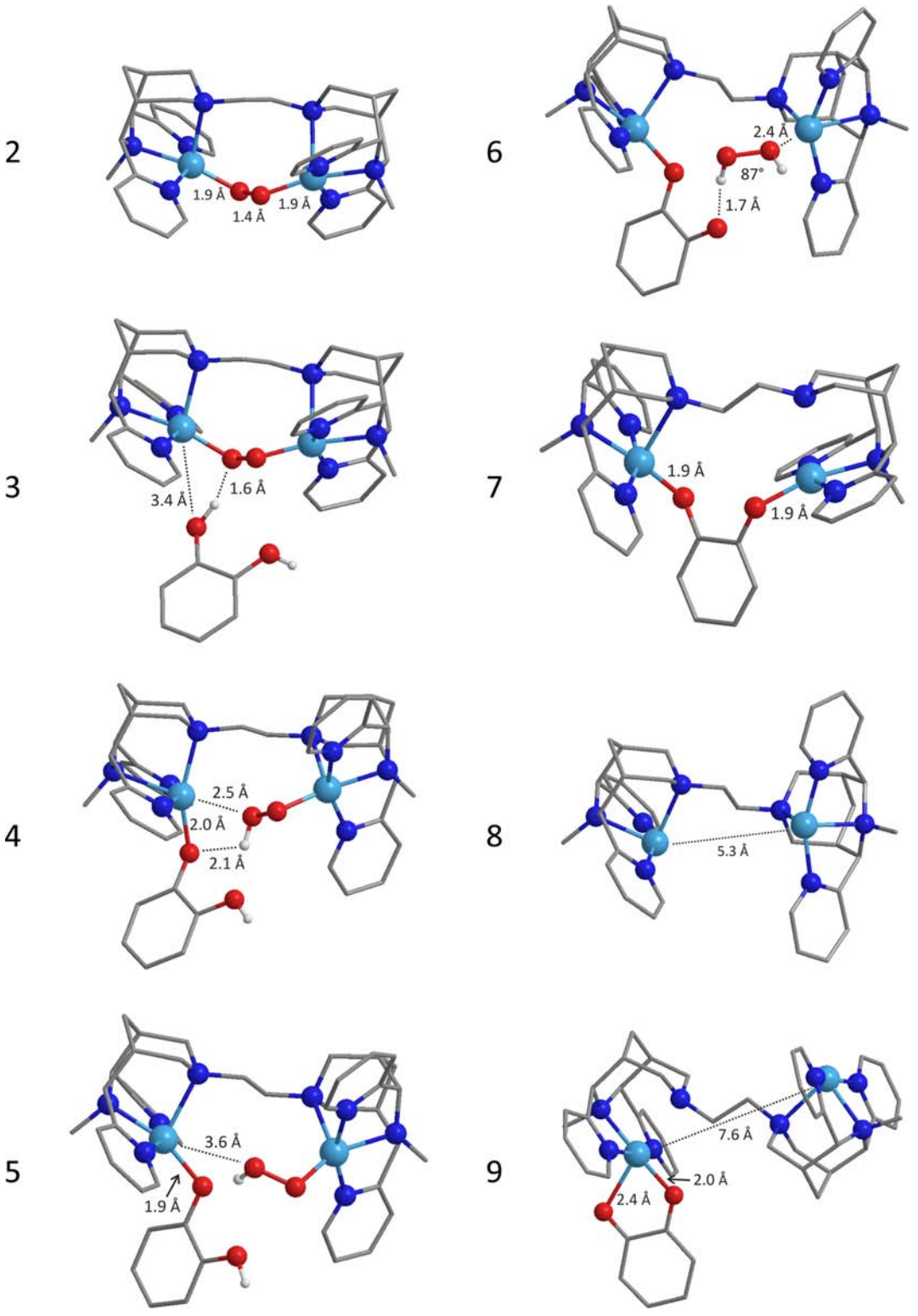

Figure 4. Optimized structures (ORCA/B1) for $S = 0$. See Scheme 3 for the structure of the bispidine ligand; color code: light blue: Cu, blue: nitrogen, red: oxygen; see Scheme 5 and Figure 3 for the numbering and description of the structures (structure 1 corresponds to structure 8); the structures for $S = 1$ are given as Supporting Information.

the *end-on*-$[Cu_2O_2]^{2+}$ active catalyst ^{3}**2**, the hydrogen atom of one of the $OH_{catechol}$ groups of the substrate interacts with the peroxo group of *end-on*-$[Cu_2O_2]^{2+}$ and forms a hydrogen-bonded weak complex ^{1}**3** which is destabilized by 3.2 kJ/mol relative to ^{3}**2** (the H···O bond distance between the catechol hydrogen and the peroxide oxygen atom is 1.63 Å, the distance of the H-bonded catechol oxygen atom to Cu^{II} is 3.37 Å). Because of this weak interaction, the corresponding $Cu-O_{peroxo}$ bond slightly elongates, from 1.90 Å in ^{3}**2** to 1.91 Å in ^{1}**3**.

In the transition state ^{3}**4**, the Cu^{II}-$O_{catecholate}$ bond shortens to 1.96 Å. The energy barrier from **3** to **5** is 27.2 kJ/mol on the $S = 1$ and 54.2 kJ/mol on the $S = 0$ surface. In the transition state

dx.doi.org/10.1021/ic3004917 | *Inorg. Chem.* 2012, 51, 9214−9225

4, the triplet is predicted to be 17.7 kJ/mol more stable than the singlet, even if ^{3}**3** is 9.3 kJ/mol less stable than ^{1}**3**. On formation of the asymmetric intermediate ^{3}**5** with a monodentate catecholate, the Cu^{II}-$O_{catecholate}$ bond shortens to 1.94 Å, while the bond between the Cu^{II} center and the protonated oxygen atom from the peroxo bridge is elongated (and virtually broken) to 3.64 Å. The energy barriers from 5 to the catecholate-bridged complex 7, involving the transition state **6**, are 89.5 kJ/mol, and 42.2 kJ/mol on the triplet and singlet surfaces, respectively. In **6**, the emerging H_2O_2 is already almost fully formed, with an average H−O distance of 0.99 Å, an O−O bond length of 1.45 Å, and a H−O−O−H dihedral of 87°. In the catecholate-bridged intermediate **7**, the $S = 0$ state is 3.8 kJ/mol more stable than the $S = 1$ state. Our calculations therefore indicate that the catalytic transformation from **2** to **7** may proceed on the open-shell singlet surface, with the exception of the transition state **4**, where the triplet state is 18 kJ/mol more stable.

At stage **7**, there is competition between two possible pathways (see also Schemes 2 and 5): a rearrangement to a dicopper(II) complex with a bidentate catecholate **9**, which is a relatively stable structure on the triplet surface (stabilization relative to **2** of 40.7 kJ/mol) and inhibits the catalytic cycle, and intramolecular transfer of two electrons in **7**, to produce the *ortho*-quinone product ^{1}**8** (39.6 kJ/mol destabilization relative to **2**), which is released from the resulting dicopper(I) complex to reform the precatalyst $[(L^2)Cu^I_2]^{2+}$ **1**. Note that the optimized structure of the inhibition product **9** has only one chelating catecholate, the second Cu^{II} center remains four-coordinate (see Figure 4). In our experimental study, we have assumed a symmetrical dicopper(II) complex with two chelating catecholate ligands (the catalytic reaction obviously was performed in an excess of catechol)[16] but coordination of a solvent molecule to complete the coordination sphere might be an alternative. Independently of the type of the additional ligand at the second Cu^{II} center, formation of **9** suffers from an additional entropy penalty, which is not included in our present analysis (see Scheme 5). That is, the relative amount of inhibition product formation is difficult to estimate but clearly smaller than appears from Figure 3. Note also that there is a possible direct pathway on the triplet surface from **6** to the inhibition product **9**, that is, coordination of catecholate as a bidentate before release of H_2O_2, and this has not been considered in our calculations.[108,109]

Nevertheless, and in contrast to the interpretation of our experimental study,[16] it appears that competition between inhibition **9** and product formation **8** is not the major or only problem of the relatively inefficient catalytic reaction.[110] The more important problem is the unprecedented stability of the peroxo-dicopper(II) complexes ^{1,3}**2**. Generally, because of significant spin density on the oxygen atoms of *end-on*-$[Cu_2O_2]$ complexes, the peroxo groups are nucleophilic and susceptible to protonation. Upon treatment with acid, these complexes generally produce H_2O_2.[37,38,111,112] Combined with the acidity of catechol (pK_a = 9.47), proton transfer and coordination of the monodeprotonated catecholate in **3**−**5**, followed by a second proton transfer and release of H_2O_2, is the expected scenario. However, with the stable *end-on*-$[(L^2)Cu_2(O_2)]^{2+}$ complex **2** studied here, with in-plane coordination of peroxide, protonation of the peroxo bridge and release of H_2O_2 is not efficient. Therefore, it is not entirely unexpected, that the overall reaction is, according to the computed free energy profile (see Figure 3), energetically unfavorable (with respect to the formation of the product **8**). This is not in full agreement with the experimental data, which show that the L^2-based copper complexes are catalytically active (see Table 2).[16] The limited accuracy of the computed energies needs to be considered,[90,113] but a main reason for the apparent inconsistency is the formation of the relatively high energy H_2O_2 side product (in comparison with H_2O which is the corresponding product in the enzymatic catalytic cycle). However, we note that H_2O_2 is unlikely to survive in presence of the dicopper(I) species in the resting state of the catalyst,[26,46] and oxidation of Cu^I by H_2O_2 (instead of O_2) has not been considered in our calculations.

CONCLUSIONS

The bis-bispidine dicopper(I) complexes discussed here are of interest because, upon oxygenation, they form *end-on*-peroxo-dicopper(II) complexes of unusual stability, and they do not rearrange to the biomimetic *side-on* isomers. Several catecholase model complexes with a *side-on*-$[Cu_2O_2]^{2+}$ core have been reported but generally there is no catalytic activity of *end-on*-$[Cu_2O_2]^{2+}$ intermediates.[112,114] The common feature of *side-on*-$[Cu_2O_2]^{2+}$ and the bispidine-based *end-on*-$[Cu_2O_2]^{2+}$ system is a $d_{x^2-y^2}$ ground state, and this might be an important condition for catalytic activity. Because of the available experimental bispidine-Cu^{II} structures with catechol coordinated in all possible modes (monodentate, bidentate, and bridging)[15] as well as the observed catecholase activity and the emerging mechanistic proposal,[16] the dinuclear copper-bispidine complexes form a unique set of compounds for a thorough analysis of bonding and reactivity of copper-dioxygen complexes. The results of the computational studies of the structures, electronics, and catalytic pathways complement the already reported experimental data as follows:

(a) The square pyramidal coordination geometry of *end-on*-$[(L^2)Cu_2(O_2)]^{2+}$, as opposed to the trigonal bipyramidal structure of other model complexes (e.g., *end-on*-$[\{(tmpa)Cu\}_2(O_2)]^{2+}$) results in a $d_{x^2-y^2}$, compared to the usually observed d_{z^2} ground state. This leads to stronger $Cu-O_{peroxo}$ σ-bonds and an increased stability of the *end-on*-$[Cu_2O_2]^{2+}$ oxygenation product.

(b) The analysis of the CT transitions of *end-on*-$[(L^2)Cu_2(O_2)]^{2+}$ [$\pi^*_\sigma \rightarrow$ Cu ($d_{x^2-y^2}$ + $d_{x^2-y^2}$) at 20,578 cm^{-1} (486 nm) and $\pi^*_v \rightarrow$ Cu ($d_{x^2-y^2}$ + $d_{x^2-y^2}$) at 15,386 cm^{-1} (650 nm)], supported by TD-DFT calculations, is in agreement with the copper−peroxo bonding analysis, that is, the $Cu-O_{peroxo}$ σ-bonding in the bispidine complexes is stronger than in model systems with the usual trigonal bipyramidal geometry.

(c) The catecholase activity of *end-on*-$[(L^2)Cu_2(O_2)]^{2+}$ is unusual and related to the $d_{x^2-y^2}$ electronic ground state. The catalytic cycle is based on a pathway which differs from that of the enzymes, that is, only one catechol is oxidized per cycle to an *ortho*-quinone, and dioxygen is reduced to H_2O_2. A similar pathway has been reported for other model complexes,[46,47] and it may also be relevant for the copper-loaded S100B protein.[115]

(d) The unusual stability of the *end-on*-[(bispidine)-$Cu_2(O_2)]^{2+}$ complex and inhibition of the catalytic transformation by a rearrangement of bridging to chelating catecholate are identified as reasons for the relatively inefficient catalytic process.

dx.doi.org/10.1021/ic3004917 | Inorg. Chem. 2012, 51, 9214−9225

■ ASSOCIATED CONTENT

Supporting Information

Comparison of $[(L^2)Cu_2(O_2)]^{2+}$ with $[(tmpa)_2Cu_2(O_2)]^{2+}$ (spin densities in both spin states); calibration of the functionals for the prediction of structures and energetics of the dicopper(II)peroxo complexes; TD DFT analysis of $[(L^2)Cu_2O_2]^{2+}$ in both spin states; computed geometries of the $[(L^2)Cu_2(O_2)]^{2+}$ complex for $S = 0$ and $S = 1$, given as *xyz* files; gas phase and solvent calculations with Gaussian 09/BS2, including ZPE-corrected free energies; overlays between the ORCA/BS1 and Gaussian09/BS2 optimized geometries. This material is available free of charge via the Internet at http://pubs.acs.org.

■ AUTHOR INFORMATION

Corresponding Author

*Fax: +49-6226-546617. E-mail: peter.comba@aci.uni-heidelberg.de.

Notes

The authors declare no competing financial interest.

■ ACKNOWLEDGMENTS

We are grateful for generous financial support by the German Science Foundation (DFG).

■ REFERENCES

(1) Kitajima, N.; Moro-oka, Y. *Chem. Rev.* **1994**, *94*, 737.
(2) Lewis, E. A.; Tolman, W. B. *Chem. Rev.* **2004**, *104*, 1047.
(3) Reedijk, J.; Bouwman, E. *Bioinorganic Catalysis*, 2nd ed.; Marcel Dekker: New York, 1999.
(4) Karlin, K. D.; Lee, D.-H.; Obias, V.; Humphreys, K. J. *Pure Appl. Chem.* **1998**, *70*, 855.
(5) Solomon, E. I.; Tuczek, F.; Root, D. E.; Brown, C. A. *Chem. Rev.* **1994**, *94*, 827.
(6) Mirica, L. M.; Ottenwaelder, X.; Stack, T. D. P. *Chem. Rev.* **2004**, *104*, 1013.
(7) Hatcher, L. Q.; Karlin, K. D. *Adv. Inorg. Chem.* **2006**, *58*, 131.
(8) Sheldon, R. A.; Kochi, J. K. *Metal-Catalyzed Oxidations of Organic Compounds*; Academic Press: New York, 1981.
(9) Jorgensen, K. A. *Chem. Rev.* **1989**, *89*, 431.
(10) Sheldon, R. A.; Arends, I.; Hanefeld, U. *Green Chemistry and Catalysis*; Wiley-VCH: Weinheim, Germany, 2007.
(11) Kaim, W.; Schwederski, B. *Bioanorganische Chemie*, 3 Aufl.; B. G. Teuber: Stuttgart, Germany, 2004.
(12) Cramer, C. J.; Tolman, W. B. *Acc. Chem. Res.* **2007**, *40*, 601.
(13) Itoh, S. *Copper-Oxygen Chemistry*; Karlin, K. D., Itoh, S., Eds.; Wiley & Sons: Weinheim, Germany, 2011; p 225.
(14) Börzel, H.; Comba, P.; Katsichtis, C.; Kiefer, W.; Lienke, A.; Nagel, V.; Pritzkow, H. *Chem.—Eur. J.* **1999**, *5*, 1716.
(15) Börzel, H.; Comba, P.; Pritzkow, H. *J. Chem. Soc., Chem. Commun.* **2001**, 97.
(16) Born, K.; Comba, P.; Daubinet, A.; Fuchs, A.; Wadepohl, H. *J. Biol. Inorg. Chem.* **2007**, *12*, 36.
(17) Gerdemann, C.; Eicken, C.; Krebs, B. *Acc. Chem. Res.* **2002**, *35*, 183.
(18) Mayer, A. M.; Harel, E. *Phytochemistry* **1979**, *18*, 193.
(19) Eicken, C.; Zippel, F.; Büldt-Karentzopoulos, K.; Krebs, B. *FEBS Lett.* **1998**, *436*, 293.
(20) Siegbahn, P. E. M. *J. Biol. Inorg. Chem.* **2004**, *9*, 577.
(21) Siegbahn, P. E. M. *Q. Rev. Biophys.* **2003**, *36*, 91.
(22) Siegbahn, P. E. M. *J. Biol. Inorg. Chem.* **2003**, *8*, 577.
(23) Gherman, B. F.; Cramer, C. J. *Coord. Chem. Rev.* **2009**, *253*, 723.
(24) Cramer, C. J.; Kinal, A.; Wloch, M.; Piecuch, P.; Gagliardi, L. *J. Phys. Chem. A* **2006**, *110*, 11557.
(25) Guell, M.; Siegbahn, P. E. M. *J. Biol. Inorg. Chem.* **2007**, *12*, 1251.
(26) Koval, I. A.; Gamez, P.; Belle, C.; Selmeczib, K.; Reedijk, J. *Chem. Soc. Rev.* **2006**, *35*, 814.
(27) Rolff, M.; Schottenheim, J.; Decker, H.; Tuczek, F. *Chem. Soc. Rev.* **2011**, *40*, 4077.
(28) Eicken, C.; Krebs, B.; Sacchettini, J. C. *Curr. Opin. Chem. Biol.* **1999**, *9*, 677.
(29) Klabunde, T.; Eicken, C.; Saccettini, J. C.; Krebs, B. *Nat. Struct. Biol.* **1998**, *5*, 1084.
(30) Bassan, A.; Borowski, T.; Siegbahn, P. E. M. *Dalton Trans.* **2004**, 3153.
(31) Note that in Scheme 2 we show one of the original proposals which has been challenged in a few details by later work, specifically from computational studies. Important here is primarily the difference with respect to the bispidine-based model reaction.
(32) Comba, P.; Hilfenhaus, P.; Karlin, K. D. *Inorg. Chem.* **1997**, *36*, 2309.
(33) Jacobson, R. R.; Tyeklar, Z.; Farooq, A.; Karlin, K. D.; Liu, S.; Zubieta, J. *J. Am. Chem. Soc.* **1988**, *110*, 3690.
(34) Karlin, K. D.; Tyeklar, Z.; Farooq, A.; Jacobson, R. R. *Inorg. Chim. Acta* **1991**, *182*, 1.
(35) Koval, I. A.; Pursche, D.; Stassen, A. F.; Gamez, P.; Krebs, B.; Reedijk, J. *Eur. J. Inorg. Chem.* **2003**, 1669.
(36) Baldwin, M. J.; Ross, P. K.; Pate, J. E.; Tyeklar, Z.; Karlin, K. D.; Solomon, E. I. *J. Am. Chem. Soc.* **1991**, *113*, 8671.
(37) Karlin, K. D.; Ghosh, P.; Cruse, R. W.; Farooq, A.; Gultneh, Y.; Jacobson, R. R.; Blackburn, N. J.; Strange, R. W.; Zubieta, J. *J. Am. Chem. Soc.* **1988**, *110*, 6769.
(38) Tyeklar, Z.; Paul, P. P.; Jacobson, R. R.; Farooq, A.; Karlin, K. D.; Zubieta, J. *J. Am. Chem. Soc.* **1989**, *111*, 388.
(39) Solomon, E. I.; Sarangi, R.; Woertink, J. S.; Augustine, A. J.; Yoon, J.; Gosh, S. *Acc. Chem. Res.* **2007**, *40*, 581.
(40) Chen, P.; Solomon, E. I. *Proc. Natl. Acad. Sci. U.S.A.* **2004**, *101*, 13105.
(41) Neves, A.; Rossi, L. M.; Bortoluzzi, A. J.; Szpoganicz, B.; Wiezbicki, C.; Schwingel, E.; Haase, W.; Ostrovsky, S. *Inorg. Chem.* **2002**, *41*, 1788.
(42) Merkel, M.; Möller, N.; Piacenzy, M.; Grimme, S.; Rompel, A.; Krebs, B. *Chem.—Eur. J.* **2005**, *11*, 1201.
(43) Ackermann, J.; Meyer, F.; Kaifer, E.; Pritzkow, H. *Chem.—Eur. J.* **2002**, *8*, 247.
(44) Kao, C.-H.; Wei, H.-H.; Liu, Y.-H.; Lee, G.-H.; Wang, Y.; Lee, C.-J. *J. Inorg. Biochem.* **2001**, *84*, 171.
(45) Mukherjee, J.; Mukherjee, R. *Inorg. Chim. Acta* **2002**, *337*, 429.
(46) Monzani, E.; Battaini, G.; Perotti, A.; Casella, L.; Gullotti, M.; Santagostini, L.; Nardin, G.; Randaccio, L.; Geremia, S.; Zanello, P.; Opromolla, G. *Inorg. Chem.* **1999**, *38*, 5359.
(47) Granata, A.; Monzani, E.; Casella, L. *J. Biol. Inorg. Chem.* **2004**, *9*, 903.
(48) Torelli, S.; Belle, C.; Gautier-Luneau, I.; Pierre, J. L.; Saint-Aman, E.; Latour, J. M.; Pape, L. L.; Luneau, D. *Inorg. Chem.* **2000**, *39*, 3526.
(49) Fernandes, C.; Neves, A.; Bortoluzzi, A. J.; Mangrich, A. S.; Rentschler, E.; Szpoganicz, B.; Schwingel, E. *Inorg. Chim. Acta* **2001**, *320*, 12.
(50) Kaizer, J.; Pap, J.; Speier, G.; Parkanyi, L.; Korecz, L.; Rockenbauer, A. *J. Inorg. Biochem.* **2002**, *91*, 190.
(51) Reim, J.; Krebs, B. *J. Chem. Soc., Dalton Trans.* **1997**, 3793.
(52) Rockcliffe, D. A.; Martell, A. E. *J. Chem. Soc., Chem. Commun.* **1992**, 1758.
(53) Rockcliffe, D. A.; Martell, A. E. *Inorg. Chem.* **1993**, *32*, 3143.
(54) Comba, P.; Lienke, A. *Inorg. Chem.* **2001**, *40*, 5206.
(55) Börzel, H.; Comba, P.; Hagen, K. S.; Kerscher, M.; Pritzkow, H.; Schatz, M.; Schindler, S.; Walter, O. *Inorg. Chem.* **2002**, *41*, 5440.
(56) Comba, P.; Kerscher, M.; Schiek, W. *Prog. Inorg. Chem.* **2007**, *55*, 613.
(57) Comba, P.; Nuber, B.; Ramlow, A. *J. Chem. Soc., Dalton Trans.* **1997**, 347.

(58) There is a second generation bispidine ligands which enforces trigonal geometries,[59] and these have a very different copper-dioxygen chemistry.[60]
(59) Comba, P.; Haaf, C.; Wadepohl, H. *Inorg. Chem.* **2009**, *48*, 6604.
(60) Comba, P.; Haaf, C.; Helmle, S.; Karlin, K. D.; Pandian, S.; Waleska, A. *Inorg. Chem.* **2012**, *51*, 2841.
(61) Neese, F. *J. Chem. Phys.* **2003**, *119*, 9428.
(62) Neese, F. *Int. J. Quantum Chem.* **2001**, *83*, 104.
(63) Becke, A. D. *J. Chem. Phys.* **1992**, *96*, 2155.
(64) Becke, A. D. *J. Chem. Phys.* **1992**, *97*, 9713.
(65) Becke, A. D. *J. Chem. Phys. B* **1993**, *98*, 5648.
(66) Schäfer, A.; Horn, H.; Ahlrichs, R. *J. Chem. Phys.* **1992**, *97*, 2571.
(67) Ahlrichs, R.; Weigand, F. *Phys. Chem.* **2005**, *7*, 3297.
(68) *Jaguar 5.5, Jaguar 6.5*; Schrödinger LLC: New York, NY, 2005.
(69) Frisch, M. J.; Trucks, G. W.; Schlegel, H. B.; Scuseria, G. E.; Robb, M. A.; Cheeseman, J. R.; Scalmani, G.; Barone, V.; Mennucci, B.; Petersson, G. A.; Nakatsuji, H.; Caricato, M.; Li, X.; Hratchian, H. P.; Izmaylov, A. F.; Bloino, J.; Zheng, G.; Sonnenberg, J. L.; Hada, M.; Ehara, M.; Toyota, K.; Fukuda, R.; Hasegawa, J.; Ishida, M.; Nakajima, T.; Honda, Y.; Kitao, O.; Nakai, H.; Vreven, T.; Montgomery Jr., J. A.; Peralta, J. E.; Ogliaro, F.; Bearpark, M.; Heyd, J. J.; Brothers, E.; Kudin, K. N.; Staroverov, V. N.; Kobayashi, R.; Normand, J.; Raghavachari, K.; Rendell, A.; Burant, J. C.; Iyengar, S.; Tomasi, J.; Cossi, M.; Rega, N.; Millam, N. J.; Klene, M.; Knox, J. E.; Cross, J. B.; Bakken, V.; Adamo, C.; Jaramillo, J.; Gomperts, R.; Stratmann, R. E.; Yazyev, O.; Austin, A. J.; Cammi, R.; Pomelli, C.; Ochterski, J. W.; Martin, R. L.; Morokuma, K.; Zakrzewski, V. G.; Voth, G. A.; Salvador, P.; Dannenberg, J. J.; Dapprich, S.; Daniels, A. D.; Farkas, O.; Foresman, J. B.; Ortiz, J. V.; Cioslowski, J.; Fox, D. J. *Gaussian 09*, Revision A.02; Gaussian, Inc.: Wallingford, CT, 2009.
(70) Dunning Jr., T. H.; Hay, P. J. *Modern Theoretical Chemistry*; Schaefer, H. F., III, Ed.; Plenum Press: New York, 1976; Vol. 3, pp 1.
(71) Hay, P. J.; Wadt, W. R. *J. Chem. Phys.* **1985**, *82*, 270.
(72) Wadt, W. R.; Hay, P. J. *J. Chem. Phys.* **1985**, *82*, 284.
(73) Grimme, S.; Ehrlich, S.; Goerigk, L. *J. Comput. Chem.* **2011**, *32*, 1456.
(74) Grimme, S.; Antony, J.; Ehrlich, S.; Krieg, H. *J. Chem. Phys.* **2010**, *132*, 154104.
(75) Neese, F. *ORCA-an ab initio, density functional and semiempirical program package*, version 2.6.35; University of Bonn: Bonn, Germany, 2008 (http://www.thch.uni-bonn.de/tc/orca/).
(76) Klamt, A.; Schürmann, G. *J. Chem. Soc., Perkin Trans. 2* **1993**, 799.
(77) Siegbahn, P. E. M.; Blomberg, M. R. A.; Chen, S.-L. *J. Chem. Theory Comput.* **2010**, *6*, 2040.
(78) Rezabal, E.; Gauss, J.; Matxain, J. M.; Berger, R.; Diefenbach, M.; Holthausen, M. C. *J. Chem. Phys.* **2011**, *134*, 064304.
(79) Dietl, N.; van der Linde, C.; Schlangen, M.; Beyer, M. K.; Schwarz, H. *Angew. Chem., Int. Ed.* **2011**, *50*, 4966.
(80) de Visser, S. P.; Ogliaro, F.; Harris, N.; Shaik, S. *J. Am. Chem. Soc.* **2001**, *123*, 3037.
(81) Bassan, A.; Blomberg, M. R. A.; Siegbahn, P. E. M. *Chem.—Eur. J.* **2003**, *9*, 4055.
(82) Bassan, A.; Blomberg, M. R. A.; Siegbahn, P. E. M. *J. Biol. Inorg. Chem.* **2004**, *9*, 439.
(83) Bassan, A.; Blomberg, M. R. A.; Siegbahn, P. E. M.; Que, L., Jr. *Chem.—Eur. J.* **2005**, *11*, 692.
(84) Quinonero, D.; Morokuma, K.; Musaev, D. G.; Morokuma, K.; Mas-Balleste, R.; L. Que, J. *J. Am. Chem. Soc.* **2005**, *127*, 6548.
(85) Harvey, J. N. *Annu. Rep. Prog. Chem., Sect. C* **2006**, *102*, 203.
(86) Siegbahn, P. E. M.; Borowski, T. *Acc. Chem. Res.* **2006**, *39*, 729.
(87) The discrepancies between the two energy levels in this particular case is as high as 90 kJ/mol; note, however, that the comparison has been made with the BLYP functional which is known to disfavor the singlet state much more than the hybrid B3LYP functional.[88,89]
(88) Benjamin, F.; Gherman, B. F.; Cramer, C. J. *Inorg. Chem.* **2004**, *43*, 7281.
(89) Ruiz, E.; Alvarez, S.; Rodriguez-Fortea, A.; Alemany, P.; Pouillon, Y.; Massobrio, C. *Magnetism: Molecules to Materials*; Wiley-VCH: Weinheim, Germany, 2001; Vol. 2, p 227.
(90) Siegbahn, P. E. M. *J. Biol. Inorg. Chem.* **2006**, *11*, 695.
(91) Atanasov, M.; Comba, P.; Martin, B.; Müller, V.; Rajaraman, G.; Rohwer, H.; Wunderlich, S. *J. Comput. Chem.* **2006**, *27*, 1263.
(92) Comba, P.; Kerscher, M. *Coord. Chem. Rev.* **2009**, *253*, 564.
(93) Neese, F. *Coord. Chem. Rev.* **2009**, *253*, 526.
(94) All data of the gas phase and solvent calculations are given in the tables or as Supporting Information.
(95) Würtele, C.; Sander, O.; Lutz, V.; Waitz, T.; Tuczek, F.; Schindler, S. *J. Am. Chem. Soc.* **2009**, *131*, 7544.
(96) Komiyama, K.; Furutachi, H.; Nagatomo, S.; Hashimoto, A.; Hayashi, H.; Fujinami, S.; Suzuki, M.; Kitagawa, T. *Bull. Chem. Soc. Jpn.* **2004**, *77*, 59.
(97) Hu, H.; Zhang, D.; Chen, Z.; Liu, C. *Chem. Phys. Lett.* **2000**, *20*, 255.
(98) Comba, P.; Hausberg, S.; Martin, B. *J. Phys. Chem. A* **2009**, *113*, 6751.
(99) Solomon, E. I.; Chen, P.; Metz, M.; Lee, S.-K.; Palmer, A. E. *Angew. Chem., Int. Ed.* **2001**, *40*, 4570.
(100) Schenker, R.; Kieber-Emmons, M. T.; Riordan, C. G.; Brunold, T. C. *Inorg. Chem.* **2005**, *44*, 1752.
(101) Blanchet-Boiteux, C.; Mouesca, J.-M. *J. Phys. Chem. A* **2000**, *104*, 2091.
(102) Please note that, as stated above, we consistently compare structures with solvent and dispersion corrections, including the peroxo complex; for the tmpa complex we use the constrained Cu-O-O-Cu dihedral structure; only for the TD-DFT calculations of the peroxo complex do we compare gas phase structures.
(103) Lehnert, N.; Cornelissen, U.; Neese, F.; Ono, T.; Noguchi, Y.; Okamoto, K.; Fujisawa, K. *Inorg. Chem.* **2007**, *46*, 3916.
(104) All computational work in this part relates to the copper complexes of the ethyl-bridged dinucleating ligand L^2 and the chemical model (see Computational Details), where the ester and keto groups in positions 1, 5, and 9 have been replaced by hydrogen atoms.
(105) Except for the transition state structure 6 (see below) this is true for the entire reaction coordinate.
(106) Shaik, S.; Danovich, D.; Fiedler, A.; Schröder, D.; Schwarz, H. *Helv. Chim. Acta* **1995**, *78*, 1393.
(107) We restrict ourselves to the description of the calculations with solvent corrections and dispersion, as for most intermediates similar structures were obtained in the gas phase calculations. Relative solvent stabilization energies for the $S = 0$ and $S = 1$ spin states are given as Supporting Information. In general, the $S = 1$ state is favored by 15−30 kJ/mol by the solvent with respect to the corresponding gas phase calculations (with Gaussian 09).
(108) Note that other pathways, involving the formation of semiquinone intermediates, have been proposed for other systems which may also lead to H_2O_2 instead of H_2O.[26,109]
(109) Selmeczi, K.; Reglier, M.; Giorgi, M.; Speier, G. *Coord. Chem. Rev.* **2003**, *245*, 191.
(110) Note, however, that formation of the relatively stable dicopper(II) complex with one or two chelating catecholate ligands, (9), removes the catalyst from the catalytic cycle, while the dicopper(I) complex (8) is efficiently reoxidized to the catalytically efficient peroxo complex (3). Formation of the inhibition product (9) is responsible for the differences observed between the L^2- and L^5-based systems,[16] and this has been confirmed by a preliminary DFT-based analysis.
(111) Paul, P. P.; Tyeklar, Z.; Jacobson, R. R.; Karlin, K. D. *J. Am. Chem. Soc.* **1991**, *113*, 5322.
(112) Koval, I. A.; Belle, C.; Selmeczi, K.; Philouze, C.; Saint-Aman, E.; Schuitema, A. M.; Gamez, P.; Pierre, J.-L.; Reedijk, J. *J. Biol. Inorg. Chem.* **2005**, *10*, 739.
(113) In general B3LYP energies are believed to be reliable within an error limit of 10−15 kJ/mol.[90] Note however, that the energies reported here are based on relatively low-level basis sets (see Computational Details). We have done single point calculations at

the B3LYP/TZPV level, albeit without frequency analyses. As the effects are relatively small, we have used the LANL2DZ-based data in our discussion.

(114) The other example of a catalytically active *end-on*-$[Cu_2O_2]^{2+}$ species is a recently reported macrocyclic ligand dicopper complex, where both *side-on* and *end-on* intermediates are proposed in the catalytic cycle.[112]

(115) Senior, S. Z.; Mans, L. L.; VanGuilder, H. D.; Kelly, K. A.; Hendrich, M. P.; Elgren, T. E. *Biochemistry* **2003**, *42*, 4392.

dx.doi.org/10.1021/ic3004917 | *Inorg. Chem.* 2012, 51, 9214−9225